



## Alkaline Microfluidic Hydrogen-Oxygen Fuel Cell as a Cathode Characterization Platform

Fikile R. Brushett,<sup>\*</sup> Wei-Ping Zhou,<sup>a</sup> Ranga S. Jayashree,<sup>b</sup> and Paul J. A. Kenis<sup>\*\*z</sup>

Department of Chemical & Biomolecular Engineering, University of Illinois at Urbana Champaign, Urbana, Illinois 61801, USA

We report on an alkaline microfluidic fuel cell for catalyst and electrode characterization. Its constantly refreshing alkaline electrolyte stream enables autonomous control over the flow rate and electrolyte composition, as well as independent analysis of the individual electrodes, rendering this platform a powerful analytical tool. Here, polytetrafluoroethylene (PTFE)-bonded Ag/C and Pt/C cathodes are investigated and optimized using several characterization techniques, including chronoamperometry and electrochemical impedance spectroscopy. A loading of 40 wt % PTFE and hot pressing of the electrodes were found to lead to the best performance. Moreover, improvements in cell performance as a function of increasing [KOH] were investigated and the dual effects of enhanced oxygen reduction reaction activity and improved ionic conductivity were decoupled. Peak power densities as high as 110 mW/cm<sup>2</sup> were obtained, suggesting that the current alkaline fuel cell configuration may also hold promise as a microscale power source.

© 2009 The Electrochemical Society. [DOI: 10.1149/1.3083226] All rights reserved.

Manuscript submitted November 11, 2008; revised manuscript received January 26, 2009. Published March 5, 2009.

Fuel cells are investigated extensively as alternative power sources because of their high efficiency and their potential to achieve high energy density.<sup>1,2</sup> One of the first successful applications of fuel cell technologies were alkaline fuel cells (AFCs) used for both vehicular studies in the 1950s and the NASA Apollo space program in the 1960s.<sup>3</sup> These AFCs used stationary potassium hydroxide (KOH) electrolyte to separate gaseous streams of hydrogen (H<sub>2</sub>) and oxygen (O<sub>2</sub>). Operating fuel cells in alkaline media, as opposed to acidic media, has the advantage of enhanced oxygen reduction reaction (ORR) kinetics, and as a result, inexpensive non-precious metals, such as silver (Ag), can be used as cathode catalysts instead of precious metals such as platinum (Pt) while accomplishing similar performances.<sup>4-8</sup>

Significant research efforts have sought to gain a better understanding of oxygen reduction electrocatalysis on Ag catalyst in alkaline media.<sup>6,9-12</sup> For example, Lima et al. reported the existence of a volcano-type dependence between the experimentally determined alkaline ORR activities of several electrocatalysts, including Ag and Pt, and the location of their calculated metal d-band center energies.<sup>12</sup> Pt is found at the top of the volcano, indicating higher ORR activity, whereas Ag is located at the bottom of the curve, indicating lower ORR activity. Blizanac et al.<sup>13</sup> and Markovic and Ross<sup>14</sup> found that oxygen reduction on Ag single crystals proceeds via a four-electron, direct reaction pathway with minimal peroxide formation, similar to the direct ORR pathway occurring on single-crystal Pt surfaces. This four-electron direct pathway is faster than various two-step indirect pathways observed on other metal surfaces.<sup>15,16</sup> Previous studies have shown that the ORR activity on Pt is significantly greater than on Ag in mild alkaline media (pH 13–14).<sup>9,12</sup> However, Chatenet et al. reported that further increasing the hydroxide concentration improved the ORR activity on Ag but not on Pt, thus making Ag catalysts more competitive in strong alkaline media (pH > 15).<sup>10</sup> Furthermore, Ag is an attractive alternative to Pt as an oxygen reduction electrocatalyst in alkaline media because carbon-supported Ag cathodes exhibit better long-term operational stability than carbon-supported Pt cathodes.<sup>7</sup>

Traditionally, the major technical concerns for operation of AFCs using stationary liquid electrolytes are water management at the

electrodes, long-term electrode durability in highly caustic environments, and carbonate formation when organic fuels such as methanol are used.<sup>4,17,18</sup> In AFCs, hydrogen is consumed and water is produced at the anode. If all the hydrogen is consumed, then no gas remains to sweep the formed water away from the anode, leading to anode flooding, which hinders hydrogen transport to catalytic sites. Additionally, at high current densities significant amounts of water are consumed at the cathode, which cannot be replenished fast enough, leading to electrode dry out. A second significant hurdle is long-term electrode degradation due to the caustic environment. For example, radical chain destruction of the hydrophobic binder polymers within the catalytic layer leads to (i) “electrode weeping,” where the electrolyte floods the entire electrode, and (ii) mechanical instability in the catalyst layer, causing catalyst leaching. A third challenge that hampers AFCs is carbonate formation through reaction of carbon dioxide (CO<sub>2</sub>) with hydroxyl ions. Carbonate-related issues are particularly acute when organic fuels are used. To a lesser extent, traces of CO<sub>2</sub> in the atmosphere can lead to a gradual performance drop when an air-breathing cathode is used. The carbonates deposit in both the electrolyte and gas-diffusion electrode (GDE) microporous structure where they hinder long-term electrode performance. Formation of carbonates over time also reduces the hydroxyl concentration in a stationary electrolyte thus gradually reducing electrode kinetics and electrolyte conductivity. Furthermore, any carbon monoxide (CO) present, either from the atmosphere, as a gaseous contaminant, or as an intermediate of organic fuel oxidation, can lead to catalyst poisoning, which also reduces performance. The above adverse effects have limited implementation of AFC technology mostly to applications where cost is less of an issue, allowing for the use of high-purity hydrogen and oxygen gas streams with CO and CO<sub>2</sub> concentrations below the ppm level.

Recently, significant efforts have been devoted to improving the performance of alkaline anion-exchange membranes (AAEM) to that of Nafion-based membranes that are typically used in acidic H<sub>2</sub>/O<sub>2</sub> fuel cells.<sup>19-23</sup> The design of suitable AAEMs is a challenging task due to the larger size of the hydroxyl ions as compared to protons, as well as the aforementioned challenges of material stability in caustic environments and carbonate formation. Varcoe et al.<sup>21</sup> investigated the performance of a H<sub>2</sub>/O<sub>2</sub> fuel cell with a previously developed radiation-grafted AAEM using polytetrafluoroethylene (PTFE)-bonded Pt/C, Ag/C, and Au/C cathodes.<sup>24</sup> Sleightholme et al.<sup>23</sup> observed better oxygen reduction kinetics at a catalyst/hydroxide-exchange membrane interface than at a catalyst/aqueous sodium hydroxide (NaOH) interface. They attribute the enhanced electrocatalytic activity at the catalyst/membrane interface to reduced oxide/hydroxide coverage on the Ag surface at high poten-

\* Electrochemical Society Student Member.

\*\* Electrochemical Society Active Member.

<sup>a</sup> Present address: Bldg. 55, Brookhaven Ave., Brookhaven National Lab, Upton, NY 11973.

<sup>b</sup> Present address: P.O. Box 4098, Chemistry Department, Georgia State University, Atlanta, GA 30302.

<sup>z</sup> E-mail: kenis@illinois.edu

tials, which provides more ORR sites.<sup>23</sup> In a recent study, others reported on the performance of a H<sub>2</sub>/air alkaline fuel cell operated with four different anion exchange membranes with both Pt/C and Ag/C cathodes.<sup>22</sup>

Despite these notable improvements to AAEMs with respect to conductivity, stability, and robustness compared to liquid alkaline electrolytes, the same membrane-related disadvantages that hamper acidic Nafion-based fuel cells, including water management issues (electrode flooding/dry out) and membrane cost, apply to AAEMs. For example, Varcoe et al. cited insufficient transport of water to cathodic reaction sites as the predominant source of performance limitations.<sup>21</sup> Additionally, the inherent alkalinity of the AAEM limits ways to fine tune the electrolyte composition with respect to optimizing electrode reaction kinetics (e.g., optimize pH). Furthermore, when contaminants due to carbonation and binder degradation build up in the membranes, the whole membrane electrode assembly needs to be replaced, whereas an AFC configuration with a liquid electrolyte allows for rapid exchange of the electrolyte as well as acid rinsing for contaminant removal.

In prior work, we have developed and characterized a microfluidic hydrogen-oxygen fuel cell with a flowing acidic electrolyte stream, which eliminates water management issues, facilitates by-product removal, and enables electrolyte flexibility (i.e., composition and concentration).<sup>25</sup> Here, we report on an alkaline microfluidic hydrogen-oxygen fuel cell for catalyst and electrode characterization. The flowing electrolyte configuration can diminish the carbonate formation issues encountered in traditional AFCs because the flow will remove any carbonates that form, a strategy that has been used in several larger scale AFCs.<sup>5,26,27</sup> For these AFCs, the researchers were interested in stabilizing and prolonging fuel cell performance as compared to traditional AFCs, which employ stationary liquid electrolytes. For analytical investigations, a flowing electrolyte stream eliminates adverse fuel cell system limitations (i.e., water management and carbonate removal), enabling unfettered analysis of electrode performance. Furthermore, autonomous control over the convecting stream enables in operando compositional flexibility without fuel cell disassembly. Moreover, by placing an external reference electrode in the exiting electrolyte stream the performance of each electrode can be independently analyzed.<sup>28</sup> Thus, the microfluidic platform reported here provides the experimental versatility of a traditional three-electrode electrochemical cell in an operating fuel cell. Here, we demonstrate the utility of the pH-tunable microfluidic design by investigating fuel cell and individual electrode performance, comparing PTFE-bonded Ag/C and Pt/C cathodes, under a wide range of experimental conditions.

### Experimental

**GDE preparation.**— Commercially available Pt/C (50% mass on Vulcan carbon, E-TEK) or Ag/C (60% mass on Vulcan carbon, E-TEK) were used as the cathode catalysts and PTFE (Aldrich) as the catalyst binder. The PTFE loading is expressed in terms of the weight percentage of PTFE to the total weight of the PTFE/catalyst mixture within the catalyst ink. Catalyst inks were prepared by mixing 2 mg of Pt/C or 6.7 mg of Ag/C and the desired amount of PTFE powder with 100  $\mu$ L of deionized water and 150  $\mu$ L of isopropyl alcohol. This catalyst ink was sonicated for 1 h to obtain a uniform mixture, which was then painted onto the hydrophobized-carbon side of a Toray carbon paper gas-diffusion layer (EFCG “S” type electrode, E-TEK) to create a GDE. The GDE was sintered under a nitrogen atmosphere at 330°C for 20 min in a preheated tube furnace (Lindberg/Blue) followed by hot pressing at a pressure of 340 psi and a temperature of 120°C.<sup>29</sup> The final catalyst loading was either 1 mg/cm<sup>2</sup> of Pt (50% mass Pt) or 4 mg/cm<sup>2</sup> of Ag (60% mass Ag) for the cathode and 1 mg/cm<sup>2</sup> of Pt (50% mass Pt) for the anode.

**Fuel cell assembly and testing.**— The cathode (Pt/C or Ag/C) and the anode (Pt/C) were placed on the opposite sides of a 2 mm thick polymethylmethacrylate (PMMA) window, such that the

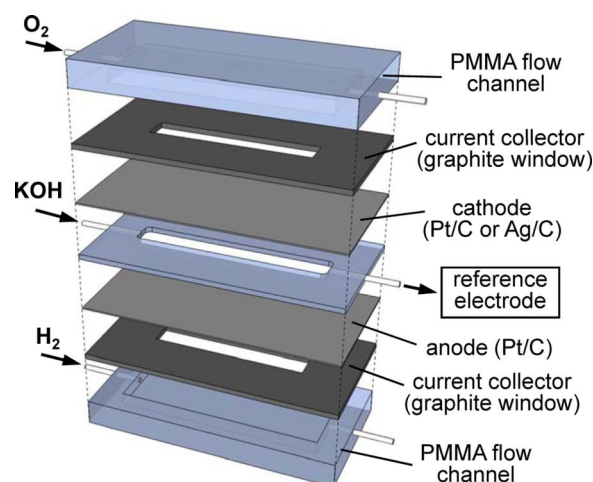


**Figure 1.** (Color online) Schematic diagram of a modular microfluidic hydrogen fuel cell with a flowing alkaline electrolyte (KOH).

catalyst-covered sides of the GDEs face the 3 cm long and 0.33 cm wide window machined in PMMA.<sup>25</sup> The window has inlets/outlets from the side for the flow of the potassium hydroxide (KOH, Aldrich) electrolyte (Fig. 1). Two 1 mm thick graphite windows were used as current collectors. The hydrogen and oxygen gas flow chambers [5 (L)  $\times$  1 (W)  $\times$  0.5 (H) cm<sup>3</sup>] were also machined into PMMA sheets. This multilayer assembly was held together with binder clips (Highmark). Fuel cell testing was conducted using a potentiostat (Autolab PGSTA-30, EcoChemie) at room temperature with hydrogen and oxygen gas (laboratory grade, S. J. Smith), each at a flow rate of 50 sccm. Electrolyte flow rates were varied from 0.0 to 0.9 mL/min using a syringe pump (Harvard Apparatus). Fuel cell polarization curves were obtained by measuring steady-state currents at different cell potentials. The exposed geometric surface area of the electrode (1 cm<sup>2</sup>) was used to calculate the current and power densities. After passing between the anode and cathode, the electrolyte stream exited the fuel cell through a plastic tube (Cole Parmer, i.d. = 1.57 mm) and was collected in a beaker. A reference electrode (Ag/AgCl in saturated NaCl, BAS) was placed in the beaker to allow for the independent analysis of polarization losses on the cathode and the anode.<sup>25,28</sup> In prior work, we have shown that this reference electrode configuration provides accurate data.<sup>28</sup> As in our previous work, no significant potential drop occurs along the plastic tubing that connects the fuel cell with the reference electrode. Moreover, use of this reference electrode allows for passive monitoring of the polarization of each electrode without affecting fuel cell performance.

**Electrochemical impedance spectroscopy (EIS).**— AC impedance spectra were recorded after obtaining current polarization curves using a frequency response analyzer controlled by a potentiostat (Autolab PGSTAT-30, EcoChemie). Impedance spectra were measured in the constant voltage mode by decreasing frequencies from 10 kHz to 30 mHz at nine points/decade. The modulating voltage was 10 mV root mean square. The impedance spectra were used to measure the internal cell resistance ( $R_{\text{cell}}$ ), including electrolyte ionic conductivity, and to measure the charge-transfer resistance ( $R_{\text{ct}}$ ) of the different cathode catalysts.

### Results and Discussion

This article presents an alkaline microfluidic hydrogen-oxygen fuel cell with a constantly refreshing electrolyte stream as a catalyst and electrode characterization platform. Here, the performances of Ag/C and Pt/C cathodes are optimized and characterized as a function of PTFE content, electrolyte composition, most notably [KOH], and electrolyte flow rate. EIS is used to investigate the

effects of electrolyte concentration on both internal cell resistance and cathodic charge-transfer resistance of the different electrodes.

*Effect of weight percentages of PTFE on fuel cell performance.*— Electrode performance depends not only on the nature and amount of the electrocatalyst used but also on electrode structure and composition, particularly the amount of hydrophobic binder. Over the past 20 years, substantial research efforts have focused on optimizing catalyst and binder loading to maximize electrode performance for traditional AFCs, phosphoric acid fuel cells, and proton exchange membrane-based fuel cells.<sup>29-34</sup> However, the current fuel cell design utilizes a flowing electrolyte stream that alters the electrode-electrolyte interface parameters. For example, the convecting alkaline electrolyte effectively addresses water management both with respect to removal of excess water formed at the anode and replenishment at the cathode. Thus, the weight percentage of PTFE binder within the painted catalyst ink must first be investigated for the system.

Both the electro-oxidation of hydrogen and the electroreduction of oxygen occur at the three-phase interface on the cathode where the oxygen/hydrogen (gas), water/electrolyte (liquid), and catalyst layer (solid) meet. The amount of PTFE in the solid layer dictates the hydrophobicity of the catalytic surface. Insufficient amounts of PTFE cause electrode flooding, which in turn hinders transport of reactant gases to the catalytic sites and lowers cell performance. Additionally, inadequate amounts of binder lead to mechanical instabilities in the GDE, including catalyst delamination or flaking under the influence of the flowing electrolyte. Conversely, excessive amounts of PTFE block catalytic sites on the electrode and increase catalyst layer hydrophobicity, which lowers catalyst performance. Furthermore, large amounts of PTFE in the catalyst layer increase GDE thickness which leads to higher ohmic and mass transport losses.<sup>35</sup> Reactant gases must travel greater distances to catalytic sites, leading to shallower concentration gradients and, consequently, lower driving forces. Hence, optimization of the catalyst ink composition is vital to maximizing cell performance.

Figure 2a shows the effects of PTFE content (i.e., 20, 30, 40, and 50 wt % PTFE) in the catalyst layers (anode and cathode) on fuel cell performance with the total Pt catalyst loading held constant at 1 mg/cm<sup>2</sup>. To avoid mass-transport limitations, the hydrogen and oxygen flow rates were both set to 50 sccm and the flow rate of the 1 M KOH electrolyte was set to 0.3 mL/min. Peak power densities of 45, 58, 83, and 41 mW/cm<sup>2</sup> were observed with the weight percentages of 20, 30, 40, and 50 wt % PTFE, respectively (Fig. 2b). The observed optimal PTFE weight percent (40 wt %) for the microfluidic hydrogen fuel cell is similar to percentages reported in the literature.<sup>29-34</sup> This PTFE loading of 40% was used for all subsequent studies.

*Effect of electrolyte flow rates.*— The effect of different electrolyte flow rates (0.0, 0.1, 0.3, and 1.0 mL/min) on the performance of a fuel cell using a Ag/C cathode was investigated, because we know from prior work that this can have a profound effect on fuel cell performance.<sup>25</sup> Prior to fuel cell testing, the Ag/C cathode was activated in the fuel cell by holding the potentiostat at 150 mA/cm<sup>2</sup> galvanostatically or 0.3 V potentiostatically for at least 20 min to reduce any Ag oxides present on the electrode surface.<sup>17</sup> Hydrogen and oxygen flow rates were both held at 50 sccm to ensure an adequate supply of fuel and oxidant.<sup>25</sup> As seen in Fig. 3, the cell performance appears insensitive to electrolyte flow rates. Even at high current densities, no mass transport limitations appear, indicating that the current fuel cell configuration is not hindered by water management issues at either electrode. Such flow-rate independence suggests that the high [KOH] provided sufficient hydroxide ion concentrations to negate any depletion gradients at the anode. Furthermore, to a lesser extent, electrode hot pressing may have improved water management (i.e., transport and balance) within the microporous gas diffusion layer.<sup>36-38</sup>

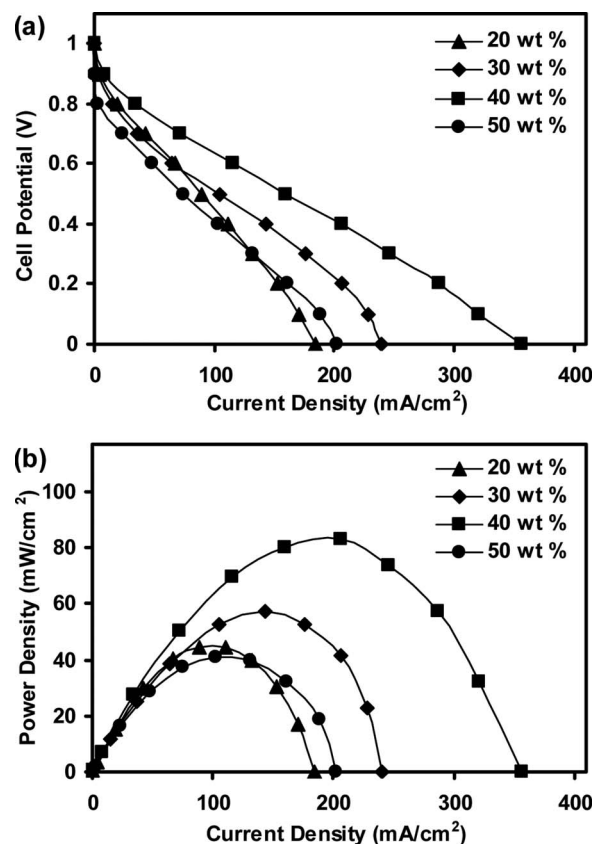


**Figure 2.** (a) Polarization curves and (b) power density curves of a microfluidic hydrogen fuel cell for electrodes with different weight percents of PTFE binder in the Pt/C catalyst layer (50% mass, 1 mg Pt/cm<sup>2</sup>). In all studies, hydrogen and oxygen flow rates were 50 sccm, the electrolyte flow rate was 0.3 mL/min, and the experiments were performed at room temperature.

*Effect of electrolyte concentration.*— Fuel cell performance with Pt/C catalyst (1 mg Pt/cm<sup>2</sup>) at the anode and Ag/C catalyst (4 mg Ag/cm<sup>2</sup>) at the cathode was also investigated as a function of KOH electrolyte concentrations (i.e., 1, 3, and 5 M KOH electrolyte streams at a flow rate of 0.3 mL/min). Figure 4a shows peak power densities of 38, 68, and 76 mW/cm<sup>2</sup> for cells operated with flowing

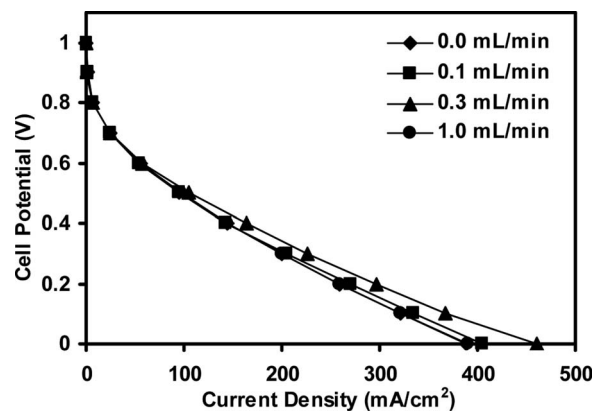


**Figure 3.** Potential polarization curves obtained for fuel cells with a Pt/C (50% mass, 1 mg Pt/cm<sup>2</sup>) anode and Ag/C (60% mass, 4 mg Ag/cm<sup>2</sup>) cathode for different electrolyte flow rates. In all these studies, the hydrogen and oxygen flow rates were 50 sccm, the KOH concentration was 3 M, and all experiments were performed at room temperature.

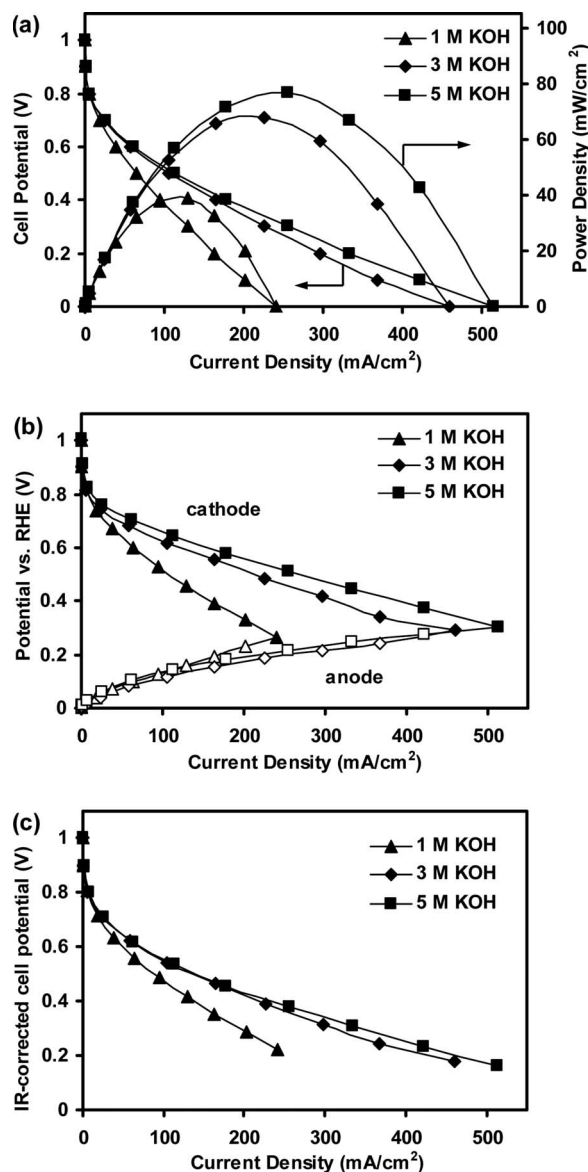


**Figure 4.** (a) Polarization and power density curves obtained with Pt/C (50% mass, 1 mg Pt/cm<sup>2</sup>) anode and Ag/C (60% mass, 4 mg Ag/cm<sup>2</sup>) cathode for different KOH electrolyte concentrations. (b) Corresponding anode and cathode polarization curves. (c) IR-corrected polarization curves for different KOH electrolyte concentrations. In all studies, hydrogen and oxygen flow rates were 50 sccm, the electrolyte flow rate was 0.3 mL/min, and the experiments were performed at room temperature.

electrolyte concentrations of 1, 3, and 5 M KOH, respectively. In Fig. 4b, the polarization curves of the individual electrodes show that the anode potential losses do not change with increasing [KOH], while the cathode potential losses decrease (i.e., improved ORR) with increasing [KOH]. The improvement in overall cell performance may be attributed to lower cell resistances<sup>25</sup> or enhanced ORR activity on Ag at higher [KOH].<sup>10</sup> Figure 4c shows the IR-corrected polarization curves to isolate the pH effect on the electrode reactions in the microfluidic fuel cell. The electrolyte solution resistances for 1, 3, and 5 M KOH are calculated to be 0.92, 0.39, and 0.32  $\Omega$ , respectively.<sup>39</sup> Compared to Fig. 4a, an enhancement in Ag oxygen reduction activity is observed between cells utilizing 1 and 3 M KOH. This indicates that both decreased solution resistances and improved cathode activity at higher [KOH] are responsible for the increase in performance. However, only minimal improvement in Ag catalytic activity is observed between cells

utilizing 3 and 5 M KOH, which suggests that a decrease in solution resistance is the main source of performance enhancement.

To further elucidate the coupled effects of [KOH] on the fuel cell performance, EIS studies were performed. Electrochemical impedance uses an alternating current of small magnitude and varying frequency to create perturbations that decouple the transport and electrode reaction phenomena associated with the overall fuel cell response.<sup>40</sup> By varying the steady-state potential at which spectra are obtained, interactions between various phenomena (i.e., cell resistances, charge-transfer resistances), which govern cell performance, may be better understood. Figures 5a-d show comparative EIS spectra for alkaline microfluidic fuel cell operated with 1, 3, and 5 M KOH recorded at four different potentials, over the range of 200–800 mV. Each set of spectra are obtained under the same experimental conditions as the polarization data shown in Fig. 4. As shown in Fig. 4b, the hydrogen oxidation reaction at the anode is unaffected by [KOH]; thus, any improvement in performance is due to improved ORR activity at the cathode or enhanced ionic conductivity. The intercept on the real Z-axis at high frequency corresponds to internal cell resistance ( $R_{\text{cell}}$ ), which includes both electrolyte solution resistance and internal cell contact resistances.<sup>41,42</sup> With increasing [KOH], this intercept value decreases, indicating lower solution resistances due to increased ionic conductivity. The diameter of the semicircular loop corresponds to the charge transfer resistance ( $R_{\text{ct}}$ ) in parallel with the double-layer capacitance ( $C_{\text{dl}}$ ).<sup>43</sup> Charge-transfer resistance is known to decrease with a decrease in cell potential due to improved electrode kinetics at higher overpotentials.<sup>10,41,43</sup> Because impedance spectra separate the effects of  $R_{\text{cell}}$  and  $R_{\text{ct}}$ , any changes in the charge-transfer resistances are due to improvements in ORR activity on the Ag cathode. Thus, these comparative studies can be used to obtain information about cathode performance. For all [KOH], a small inductance loop is observed at low frequencies that changes slightly with varying cell potentials. This feature can be linked to the relaxation of intermediate species in the multistep ORR mechanism.<sup>41,43</sup> At high potentials (low currents) on Ag catalysts, the oxygen reduction rate is low and the coverage of the intermediate species may vary, affecting the rate-determining steps of the reaction mechanism and resulting in a small negative loop. Genies et al. reported similar EIS results for the ORR on Pt/C embedded in a PTFE layer in alkaline media.<sup>41</sup> To better understand the effects of [KOH] on ORR kinetics for Ag and Pt electrocatalysts, the semicircular loop was fitted by a cell resistance ( $R_{\text{cell}}$ ) in series with a parallel  $R_{\text{ct}}-C_{\text{pe}}$  equivalent circuit. To account for the porous, distributed nature of the GDEs, a constant phase element capacitance,  $C_{\text{pe}}$ , was used to replace the  $C_{\text{dl}}$  in the curve fitting following prior work by Varcoe et al.<sup>21</sup>

Table I shows resistances and current densities obtained from the comparative EIS spectra (Fig. 5) for each electrolyte concentration at two different cell potentials, 400 and 800 mV. As expected, the electrolyte solution resistance and, consequently, the overall cell resistance decrease with increasing [KOH]. At constant [KOH],  $R_{\text{ct}}$  decreases with lowering cell potentials due to faster oxygen reduction kinetics at higher overpotentials. Interestingly, when comparing the  $R_{\text{ct}}$  at the same cell potential but different [KOH],  $R_{\text{ct}}$  decreases significantly when [KOH] changes from 1 to 3 M, and then decreases only slightly upon [KOH] further increasing from 3 to 5 M. Therefore, the enhancement in cell performance with increased electrolyte concentrations is not only due to lower ohmic potential losses in the electrolyte, but also due to the improved ORR kinetics on Ag at [KOH]  $\geq$  3 M. This result confirms the IR-corrected polarization curves in Fig. 4c and is in agreement with prior studies.<sup>10</sup> In summary, the cathode studies not only demonstrate the pH sensitivity of the ORR on Ag catalyst but also highlight the alkaline microfluidic fuel cell as a powerful and accurate electrode characterization platform.

**Cell performance with Ag or Pt cathode catalysts.**— Figure 6a shows the polarization and power density curves of fuel cells using two different cathode catalysts: 1 mg/cm<sup>2</sup> Pt and 4 mg/cm<sup>2</sup> Ag. The

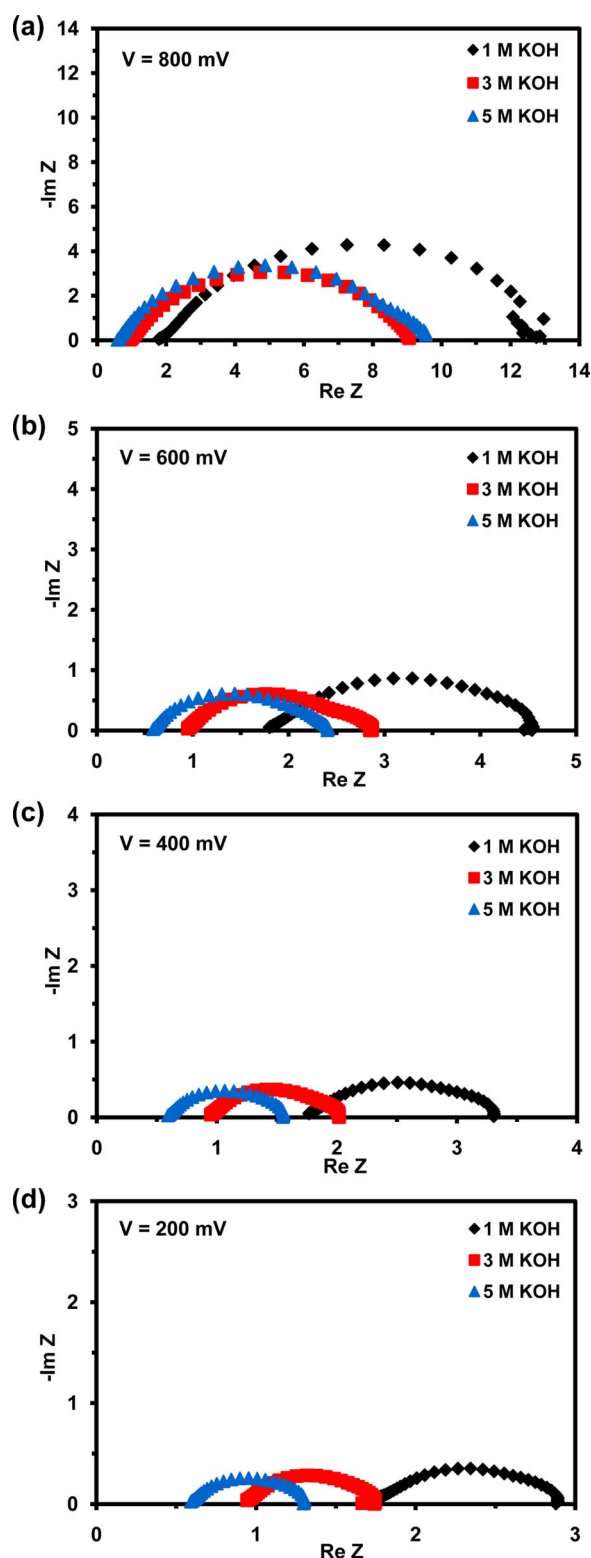


**Figure 5.** (Color online) EIS spectra of a microfluidic hydrogen fuel cell with a Pt/C (50% mass, 1 mg Pt/cm<sup>2</sup>) anode and a Ag/C (60% mass, 4 mg Ag/cm<sup>2</sup>) cathode for different KOH concentrations and different cell potentials.

comparative studies were performed using 3 M KOH as the electrolyte, flowing at 0.3 mL/min. Room-temperature peak power densities of 108 and 68 mW/cm<sup>2</sup> were observed for Pt- and Ag-based cathodes, respectively. The individual electrode polarization curves

**Table I.** Cell potentials ( $E$ ), current densities ( $j$ ), and impedance parameters for fuel cells with Pt (1 mg/cm<sup>2</sup>) as the anode and Ag (4 mg/cm<sup>2</sup>) as the cathode at two different potentials and three KOH electrolyte concentrations (all at room temperature).

[KOH] (M)	$E(E_{IR, corr})$ (mV)	$j$ (mA/cm <sup>2</sup> )	$R_{ct}$ ( $\Omega$ /cm <sup>2</sup> )	$R_{cell}$ ( $\Omega$ /cm <sup>2</sup> )
1	800 (-810)	5.6	11.3	1.76
3	800 (-806)	6.1	8.04	0.95
5	800 (-804)	6.4	8.16	0.59
1	400 (-567)	95	1.61	1.76
3	400 (-556)	164	0.99	0.95
5	400 (-505)	178	0.93	0.59

for both systems (Fig. 6b) indicate that the reduced cell performance observed with the Ag/C cathode is due to increased cathodic potential losses as compared to the Pt/C cathode. Figure 7 shows Nyquist plots of comparative EIS studies for the cells with Pt/C or Ag/C cathode catalysts at potentials of 800 and 400 mV under identical experimental conditions to Fig. 6. As shown in Fig. 6b, the hydrogen oxidation reaction is unaffected by the nature of the cathode catalyst; thus, any change in charge-transfer resistance can be attributed to the enhanced oxygen reduction activity of either Pt or Ag. The spectral features obtained with Pt/C cathode catalysts are qualitatively similar to those obtained with Ag/C cathode catalysts. How-

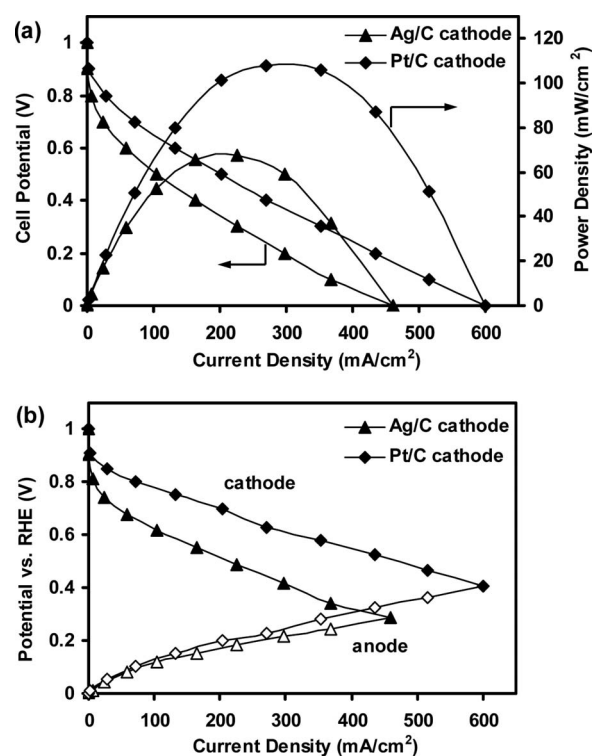


**Figure 6.** (a) Polarization and power density curves obtained for fuel cells with a Pt/C (50% mass, 1 mg Pt/cm<sup>2</sup>) anode and a Pt/C (50% mass, 1 mg Pt/cm<sup>2</sup>) or a Ag/C (60% mass, 4 mg Ag/cm<sup>2</sup>) cathode. (b) Corresponding anode and cathode polarization curves. In all studies, hydrogen and oxygen flow rates were 50 sccm, the 3 M KOH electrolyte flow rate was 0.3 mL/min, and the experiments were performed at room temperature.

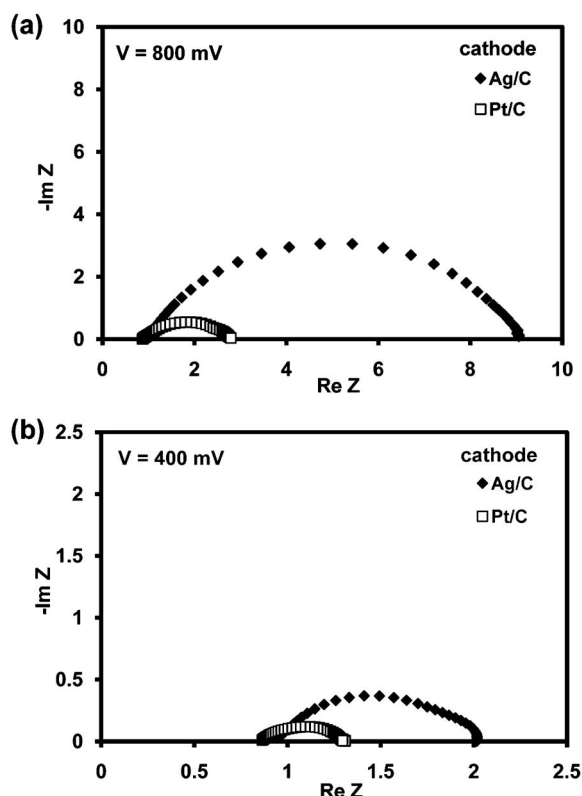


**Figure 7.** EIS spectra obtained for fuel cells with a Pt/C (50% mass, 1 mg Pt/cm<sup>2</sup>) anode and a Pt/C (50% mass, 1 mg Pt/cm<sup>2</sup>) or a Ag/C (60% mass, 4 mg Ag/cm<sup>2</sup>) cathode for potentials of (a) 800 and (b) 200 mV. In all studies, hydrogen and oxygen flow rates were 50 sccm, the 3 M KOH electrolyte flow rate was 0.3 mL/min, and the experiments were performed at room temperature.

ever, at both potentials, the  $R_{ct}$  values are lower for Pt/C cathodes than for Ag/C cathodes (Table II), indicating that even at higher [KOH], the ORR kinetics on Pt are faster than on Ag.

The peak power densities obtained in the cell configuration reported here, 108 mW/cm<sup>2</sup> with a carbon-supported Pt/C cathode (1 mg/cm<sup>2</sup> Pt) and 68 mW/cm<sup>2</sup> with a carbon-supported Ag cathode (4 mg/cm<sup>2</sup> Ag), compare favorably to values reported in literature for other alkaline fuel cells.<sup>21,22,24,44</sup> Using a H<sub>2</sub>/O<sub>2</sub> fuel cell with a radiation grafted AAEM, Varcoe et al. reported power densities of 55 and 47 mW/cm<sup>2</sup> using Pt/C (0.5 mg/cm<sup>2</sup> Pt) and Ag/C (4 mg/cm<sup>2</sup> Ag) cathodes, respectively, for a fuel cell operated at 50°C with high gas flow rates of 2000 sccm.<sup>21</sup> More recently, the same authors reported that upon further AAEM and cathode archi-

ture optimization, fuel cell performances up to 125 mW/cm<sup>2</sup> can be obtained using a Pt/C (0.55 mg/cm<sup>2</sup> Pt) cathode.<sup>44</sup> Moreover, Park et al. investigated the performance of a H<sub>2</sub>/air fuel cell operated at 60°C with four different AAEMs observing peak power densities of 28.2 and 30.1 mW/cm<sup>2</sup> for Pt/C (0.2 mg/cm<sup>2</sup> Pt) and Ag/C (0.8 mg/cm<sup>2</sup> Ag) cathodes, respectively.<sup>22</sup> It should be noted that the alkaline microfluidic fuel cell studied here has not been optimized for performance (for example, by optimizing gas and electrolyte flow fields or operation at elevated temperature), leaving room for further investigation of this configuration as a potential microscale power source.

## Conclusions

The alkaline microfluidic hydrogen-oxygen fuel cell reported in this article has proven to be an elegant electrode characterization platform. It allows for characterization of electrodes in an actual fuel cell while also allowing for electrochemical characterization of the individual electrodes within the same cell. The constantly refreshing electrolyte stream eliminates water management issues, facilitates by-product removal, and enables flexibility in electrolyte composition. Independent control of electrolyte parameters makes the microfluidic fuel cell a powerful analytical device.

Here we used this platform to characterize and optimize GDEs with PTFE-bonded Ag/C and Pt/C catalysts in alkaline media. Optimal performance was observed for hot-pressed electrodes with a 40 wt % PTFE loading. Investigation of individual Ag/C cathodes at varying electrolyte concentration revealed that cell performance improved significantly when [KOH] increased from 1 to 3 M and then improved only slightly upon [KOH] further increasing from 3 to 5 M. IR-corrected polarization curves and EIS spectra confirmed significant enhancement in Ag oxygen reduction activity at higher [KOH]. Thus, at higher [KOH], inexpensive Ag/C cathodes become an increasingly viable alternative to Pt/C cathodes.

We have demonstrated the utility of an alkaline microfluidic hydrogen-oxygen fuel cell as a catalyst/electrode characterization platform and potentially also as a microscale power source. As alkaline membrane technology continues to develop rapidly, AAEM-based H<sub>2</sub>/O<sub>2</sub> fuel cells are well on their way to becoming valid alternatives to Nafion-based H<sub>2</sub>/O<sub>2</sub>.<sup>19</sup> Stable alkaline membranes will increase the energetic efficiency (facile ORR kinetics) and reduce the cost (inexpensive catalysts) of fuel cells, improving their potential for commercial application. However, the use of organic fuels (i.e., methanol, formic acid) remains a tremendous challenge for AAEM-based fuel cell configurations due to carbonation issues. Flowing liquid electrolyte configurations remain a more feasible option for direct liquid alkaline fuel cells.

The peak power densities obtained from our current unoptimized alkaline microfluidic cell compare favorably to values reported in the literature. By optimizing electrolyte flow fields to minimize ancillary losses, introducing passive vaporized organic fuel delivery systems, and further investigating nonprecious metal electrodes, such a configuration may hold significant promise as portable power sources. Additionally, if operating the cell as a catalyst/electrode characterization tool, the introduction of a circulating alkaline electrolyte will enable long-term electrode durability studies. Of particular utility will be studying the long-term effects of carbonate formation in electrode structure (i.e., air-breathing cathodes, anodes with poisoned H<sub>2</sub> streams) and the time-dependent effects of caustic environment on electrode structure and performance (i.e., soluble degradation by-products).

## Acknowledgments

We gratefully acknowledge financial support from the Department of Energy (grant no. DE-FG02005ER46260) the National Science Foundation (Career grant no. CTS 05-47617), and a GEM Fellowship for F.R.B.

University of Illinois at Urbana Champaign assisted in meeting the publication costs of this article.

**Table II.** Cell potentials ( $E$ ), current densities ( $j$ ), and impedance parameters for fuel cells with different cathode catalysts (all Pt/C anodes) at two different potentials and 3 M KOH electrolyte (all at room temperature).

Electrodes	$E(E_{IR\ corr})$ (mV)	$j$ (mA/cm <sup>2</sup> )	$R_{ct}$ ( $\Omega$ /cm <sup>2</sup> )	$R_{cell}$ ( $\Omega$ /cm <sup>2</sup> )
Ag/C cathode	800 (-806)	6.1	8.04	0.95
Pt/C cathode	800 (-825)	28.8	1.93	0.86
Ag/C cathode	400 (-556)	164	0.99	0.95
Pt/C cathode	400 (-632)	270	0.53	0.86

## References

1. C. Apblett, D. Ingersoll, P. Atanassov, D. Maricle, and S. Sarangapani, *J. Power Sources*, **162**, 255 (2006).
2. L. Carrette, K. A. Friedrich, and U. Stimming, *ChemPhysChem*, **1**, 162 (2000).
3. S. Supramaniam, *Fuel Cells: From Fundamentals to Applications*, p. 196, Springer, New York (2006).
4. G. F. McLean, T. Niet, S. Prince-Richard, and N. Djilali, *Int. J. Hydrogen Energy*, **27**, 507 (2002).
5. E. Gülzow, *J. Power Sources*, **61**, 99 (1996).
6. H. K. Lee, J. P. Shim, M. J. Shim, S. W. Kim, and J. S. Lee, *Mater. Chem. Phys.*, **45**, 238 (1996).
7. J. S. Spindelov and A. Wieckowski, *Phys. Chem. Chem. Phys.*, **9**, 2654 (2007).
8. C. Coutanceau, L. Demarconnay, C. Lamy, and J. M. Leger, *J. Power Sources*, **156**, 14 (2006).
9. L. Demarconnay, C. Coutanceau, and J. M. Leger, *Electrochim. Acta*, **49**, 4513 (2004).
10. M. Chatenet, L. Genies-Bultel, M. Aurousseau, R. Durand, and F. Andolfatto, *J. Appl. Electrochem.*, **32**, 1131 (2002).
11. F. H. B. Lima, J. F. R. de Castro, and E. A. Ticianelli, *J. Power Sources*, **161**, 806 (2006).
12. F. H. B. Lima, J. Zhang, M. H. Shao, K. Sasaki, M. B. Vukmirovic, E. A. Ticianelli, and R. R. Adzic, *J. Phys. Chem. C*, **111**, 404 (2007).
13. B. B. Blizanac, P. N. Ross, and N. M. Markovic, *J. Phys. Chem. B*, **110**, 4735 (2006).
14. N. M. Markovic and P. N. Ross, *Surf. Sci. Rep.*, **45**, 121 (2002).
15. S. Supramaniam, *Fuel Cells: From Fundamentals to Applications*, p. 239, Springer, New York (2006).
16. J. W. Kim and A. A. Gewirth, *J. Phys. Chem. B*, **110**, 2565 (2006).
17. E. Gülzow, *Fuel Cells*, **4**, 251 (2004).
18. M. A. Alsaleh, S. Gultekin, A. S. Alzakri, and H. Celiker, *J. Appl. Electrochem.*, **24**, 575 (1994).
19. J. R. Varcoe and R. C. T. Slade, *Fuel Cells*, **5**, 187 (2005).
20. J. R. Varcoe, R. C. T. Slade, and E. Lam How Yee, *Chem. Commun. (Cambridge)*, **13**, 1428 (2006).
21. J. R. Varcoe, R. C. T. Slade, G. L. Wright, and Y. L. Chen, *J. Phys. Chem. B*, **110**, 21041 (2006).
22. J. S. Park, S. H. Park, S. D. Yim, Y. G. Yoon, W. Y. Lee, and C. S. Kim, *J. Power Sources*, **178**, 620 (2008).
23. A. E. S. Sleightholme, J. R. Varcoe, and A. R. Kucernak, *Electrochem. Commun.*, **10**, 151 (2008).
24. J. R. Varcoe and R. C. T. Slade, *Electrochem. Commun.*, **8**, 839 (2006).
25. R. S. Jayashree, M. Mitchell, D. Natarajan, L. J. Markoski, and P. J. A. Kenis, *Langmuir*, **23**, 6871 (2007).
26. M. Cifraín and K. V. Kordesch, *J. Power Sources*, **127**, 234 (2004).
27. P. Gouerec, L. Poletto, J. Denizot, E. Sanchez-Cortezon, and J. H. Miners, *J. Power Sources*, **129**, 193 (2004).
28. E. R. Choban, P. Waszczuk, and P. J. A. Kenis, *Electrochem. Solid-State Lett.*, **8**, A348 (2005).
29. M. Ghouse, A. Alboeiz, H. Abaoud, and M. Algarni, *Int. J. Hydrogen Energy*, **20**, 727 (1995).
30. J. Kivisaari, J. Lamminen, M. J. Lampinen, and M. Viitanen, *J. Power Sources*, **32**, 233 (1990).
31. V. A. Paganin, E. A. Ticianelli, and E. R. Gonzalez, *J. Appl. Electrochem.*, **26**, 297 (1996).
32. N. Wagner, M. Schulze, and E. Gülzow, *J. Power Sources*, **127**, 264 (2004).
33. E. Gülzow, N. Wagner, and M. Schulze, *Fuel Cells*, **3**, 67 (2003).
34. D. R. Desena, E. A. Ticianelli, and E. R. Gonzalez, *J. Electroanal. Chem.*, **357**, 225 (1993).
35. S. L. A. Dasilva and E. A. Ticianelli, *J. Electroanal. Chem.*, **391**, 101 (1995).
36. A. Bazylak, D. Sinton, Z. S. Liu, and N. Djilali, *J. Power Sources*, **163**, 784 (2007).
37. P. K. Sinha, P. P. Mukherjee, and C. Y. Wang, *J. Mater. Chem.*, **17**, 3089 (2007).
38. H. Li, Y. H. Tang, Z. W. Wang, Z. Shi, S. H. Wu, D. T. Song, J. L. Zhang, K. Fatih, J. J. Zhang, H. J. Wang, et al., *J. Power Sources*, **178**, 103 (2008).
39. G. Prentice, *Electrochemical Engineering Principles*, p. 16, Prentice Hall, Englewood Cliffs, NJ (1991).
40. A. J. Bard and L. R. Faulkner, *Electrochemical Methods: Fundamentals and Applications*, p. 368, John Wiley & Sons, Hoboken, NJ (2001).
41. L. Genies, Y. Bultel, R. Faure, and R. Durand, *Electrochim. Acta*, **48**, 3879 (2003).
42. M. Eikerling and A. A. Kornyshev, *J. Electroanal. Chem.*, **475**, 107 (1999).
43. Y. Bultel, L. Genies, O. Antoine, P. Ozil, and R. Durand, *J. Electroanal. Chem.*, **527**, 143 (2002).
44. C. Tamain, S. A. Poynton, R. C. T. Slade, B. Carroll, and J. R. Varcoe, *J. Phys. Chem. C*, **111**, 18423 (2007).